Journal Name

ARTICLE

On-demand, magnetic hyperthermia-triggered drug delivery: optimisation for the GI tract

Laili Che Rose,[a,f] Joseph C. Bear,[b] Paul Southern,[c] Paul D. McNaughter,[a] R. Ben Piggott,[d] Ivan P. Parkin,[b] Sheng Qi,[e] Brian P. Hills[d,†] and Andrew G. Mayes[a]*

An orally-administered vehicle for targeted, on-demand drug delivery to the gastrointestinal (GI) tract is highly desirable due to the high instances of diseases of that organ system and harsh mechanical and physical conditions any such drug delivery vehicle has to endure. To that end, we present an iron oxide nanoparticle/wax composite capsule coating that protects the capsule contents from the highly variable chemical conditions of the GI tract. It can be triggered using magnetic hyperthermia initiated from an external AC magnetic field. The coating is produced from pharmaceutically approved materials and is applied using a simple dip-coating process using a gelatin drug capsule as a template. We show that the coating is impervious to chemical conditions found within the GI tract, but is completely melted within two minutes of hyperthermic heating under biologically-relevant conditions of temperature, pH, buffer and external field strength, allowing the delivery and dispersal of the capsule contents. The overall simplicity of action, durability and non-toxic and inexpensive nature of our drug delivery vehicle demonstrated herein are key for successful drug delivery systems for the kinds of focal therapy being sought for modern precision medicine.

Introduction

Targeted drug delivery in the gastrointestinal (GI) tract is by far the most effective and least invasive methods for the treatment for diseases ranging from Crohn's disease and irritable bowel syndrome to metastatic cancers.[1–4] Most systems involving the use of nanomaterials have focussed on intravascular delivery, with targeting augmented by close, invasive proximity injection to a diseased site or *via* attached molecular targeting moieties such as proteins.[5–8] Limitations placed on nanoparticulate intravascular delivery require individual nanoparticles to have a hydrodynamic radius of less than ~ 20 nm to avoid clearance by the Reticuloendothelial system (RES) to the liver for detoxification and removal.[9,10] The use of "stealth" nanoparticle surface coatings such as poly(ethylene glycols) have been employed to circumvent RES clearance, with mixed results.[11–14]

The use of nanocomposites in the drug delivery role has sparked fresh insights and developments. The majority of these nanocomposites are based on polymer-nanoparticle motifs, due to their ease of synthesis, self-assembly and the diverse range of polymers, nanoparticles and composite properties available.[15–18] Nanoparticles may have particular advantages in delivery to the diseased GI tract, due to their propensity to accumulate in inflamed tissues[19-20].

Many approaches for controlled drug delivery to and via the GI tract have been developed over the last decades and these have been widely investigated and reviewed[21-23]. Technologies span the range from simple environmentally controlled (e.g. acid insoluble coatings to protect tablets or capsules in the stomach), through coatings that can be hydrolysed by enzymes from commensal micro-organisms in the bowel to slow-eroding coatings to give temporal protection during transit and complex pulsatile capsule devices containing drug reservoirs and osmotic pumps designed to provide sustained delivery of drug, which have recently been reviewed by Kasekar *et al.*[24].

Although many of these approaches are highly successful and commercially exploited, all have inherent uncertainty due to the environmental and temporal variations in the gut physiology of different individuals and none is truly an externally-triggered "on-demand" delivery device with the precision to deliver its payload to a specific area within the target organ. For this type of triggered system, mechanisms for drug release have been varied in nanocomposites- from release by simple changes in pH,[25–27] to X-Ray induced nanoparticle-DNA cleavage at the opposite extreme.[28] It is desirable to have a release mechanism that can be induced on demand, with little

a. *School of Chemistry, University of East Anglia, Norwich Research Park, Norwich. NR4 7TJ, UK. *E-mail: andrew.mayes@uea.ac.uk*

b. *Department of Chemistry, University College London, 20 Gordon Street, London. WC1H 0AJ, UK.*

c. *UCL Healthcare Biomagnetics Laboratories, Royal Institution of Great Britain, 21 Albemarle Street, London, W1S 4BS, UK.*

d. *Institute of Food Research, Norwich Research Park, Colney, Norwich, NR4 7UA, UK.*

e. *School of Pharmacy, University of East Anglia, Norwich Research Park, Norwich. NR4 7TJ, UK.*

f. *School Of Fundamental Science, Universiti Malaysia Terengganu, 21030 Kuala Terengganu,Terengganu Darul Iman, Malaysia.*

† This paper is dedicated to the memory of Dr. Brian Philip Hills.

ARTICLE

to no side-effects for the patient such as tissue damage or invasive processes.[6,25,28–30] To that end, magnetic hyperthermia is a viable and effective method for on-demand drug release, with little to no side effects felt by patients when used therapeutically for magnetic fluid hyperthermia (MFH), which requires much higher field strengths and intensities for completion compared with those required for drug release.[31–35]

The conditions in the GI tract are chemically and physically harsher than those experienced by intravascular drug delivery systems.[36,37] To that end, any drug delivery system for use in the GI tract must be: impervious to changes in pH and enzyme-induced breakdown, resistant to mechanical attrition [in the stomach] and be able to be administered orally or rectally. It is also desirable that the capsule, after rupture and release, be excreted in the patient's stool. In this way, uptake of nanomaterials into the bloodstream and potential retention in the liver is largely avoided.

The system we propose utilises a resistant wax- layer, embedded with superparamagnetic iron oxide nanoparticles (SPIONs), coated on a gelatin capsule. The iron oxide nanoparticles allow for magnetic hyperthermia induced release on-demand, i.e. when a desired location is reached in the GI tract. Once activated, the magnetic nanoparticles would heat their waxy matrix, inducing melting and subsequent capsule rupture on exposure via water ingress *in vivo*. The process is summarised in scheme 1. The use of iron oxide magnetic nanoparticles has added advantages as they could be tracked *in vivo* by MRI (due to their excellent T_2 contrast)[38] and targeted without the use of molecular conjugates simply by *ex vivo* magnetic field gradients. The reagents required for the synthesis are all pharmaceutically approved for other medical uses[39] and magnetic hyperthermia frequency and field strength required are well within the accepted therapeutic limits.[40,41] This paper documents the evaluation of materials for the capsule coating and the viability of magnetic-field induced hyperthermia as the release trigger, with a discussion on magnetic hyperthermia heating of iron oxide nanoparticles at the solid / liquid phase boundary. The capsule's integrity in conditions designed to simulate the harsh physical and chemical conditions experienced in the GI tract is also explored.
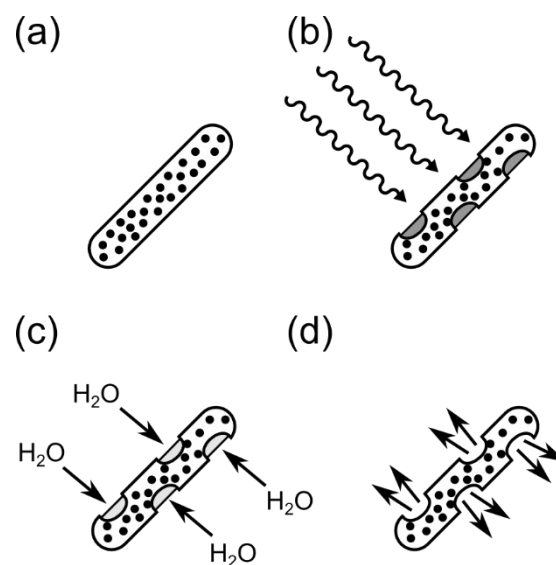
Scheme 1: The process of capsule exposure and drug release. a) SPION-wax composite coated capsule, b) radio-frequency heating causes melting and holes in the coating and exposure of the capsule to the surrounding environment, c) fluid ingress causes capsule dissolution and therefore d) drug release.

Experimental

Materials

Iron(II) sulphate heptahydrate (99 + %), iron(III) chloride hexahydrate (97 %) were purchased from Alfa Aesar. Bromo-cresol green was purchashed from BDH®. Sodium hydroxide pellets (Analytical reagent grade) and ammonium hydroxide solution (28 % in water) were purchased from Fisher Scientific Limited. Docosane (99 %), lauric acid (≥ 99 %), myristic acid (≥ 99 %), eicosane (99 %), lecithin (for microbiology), sodium dihydrogen phosphate (BioXtra, ≥ 99.0 %), sodium chloride (BioXtra, ≥ 99.5 %), bile salts (for microbiology) and paracetamol were purchased from Sigma Aldrich Limited and used as received. FaSSIF (Fasted state simulated intestinal fluid) buffer was prepared by dissolving bile salts (3 mM), lecithin (0.75 mM), sodium chloride (105.85 g) and sodium dihydrogen phosphate (28.65 g) were dissolved in deionised water (1 L). The pH was adjusted using sodium hydroxide / HCl solutions. Laboratory solvents were purchased from Sigma Aldrich or Fisher and of analytical grade or better. Aqueous solutions were prepared using UHQ deionised water with a resistivity of not less than 18.2 MΩ cm^{-1}.

Synthesis of iron oxide nanoparticles

Iron oxide nanoparticles were synthesised according to the modified protocol developed by López-López et al.[42] Briefly, a 0.72 mol dm^{-3} aqueous solution of iron(III) chloride hexahydrate was mixed with a 0.32 mol dm^{-3} aqueous solution of iron(II) sulphate heptahydrate in a molar ratio of 1:2 in a nitrogen purged reactor. Ammonium hydroxide solution was added under vigorous stirring in order to achieve a pH of 10, before addition of oleic acid (10 mL, 31.5 mmol). The dark brown suspension was subsequently heated to 95 °C, before cooling naturally to room temperature. The nanoparticles were precipitated by addition of 1 mol dm^{-3} HCl solution. The liquid was decanted, before isolation of the nanoparticles from residual reaction mixture by centrifugation (1000 × g). The pellet was re-suspended and washed with 3 × 100 mL portions of deionised water and 3 × 100 mL portions ethanol respectively. Finally, the precipitate was dried in a vacuum desiccator.

Capsule coating procedure

Dried nanoparticles were dispersed in wax mixtures by melting the wax in a beaker in a heated water bath, set about 5 °C above the melting point of the mixture, and shear mixed with an Ultra-Turrax microhomogeniser with a S5N1 dispersing head until it was homogeneous. The nanoparticle-eicosane layer was applied to the capsules by dip-coating a gelatin capsule, held on the end of a suction tube connected to a vacuum pump, into an homogenised molten suspension of 10 wt. % iron oxide nanoparticles in molten eicosane, docosane, eicosane-docosane or a fatty acid mixture. A complete coating was achieved by waiting for the molten layer to cool in ambient air before reversing the capsule to coat the second end with a small overlap in the centre to ensure complete coverage. The process was repeated for the addition of subsequent layers up to a total of three layers (1.85 mm thickness). For some studies, T-type thermocouples were embedded in the wax layer at the final coating step.

Dye release studies

Capsules were loaded with bromo-cresol green dye or paracetamol as dry powders by weighing (~ 20 mg), before closing the capsules and coating with wax layers (see previous section). Stomach fluid was simulated using HCl (pH 1.2). FaSSIF buffer was prepared according to Dressman et al.[43] Dissolution testing was carried out by submerging a coated capsule in FaSSIF buffer at 37°C in a stainless steel basket. The different pH values experienced in the GI tract were simulated by incubating the capsule first in simulated stomach acid (HCl, pH 1.2 for 2 hours), then transferring to FaSSIF buffer.

Magnetic hyperthermia testing

The propensity of the magnetic nanoparticles to heat the wax composites was tested using small bulk samples of the composites in Eppendorf tubes into which T-type thermocouples were inserted. Melting of wax coatings and rupture of the capsule in air and in fluid was evaluated by melting the capsule coatings using a water-cooled magnetic hyperthermia coil which gave specific field strengths and [radio] frequencies (vide infra). The capsule either had a glass fibre-optic thermocouple placed against the outer layer or a standard T-type thermocouple embedded in its outer layer to monitor temperature, or the whole system was monitored using a thermal imaging camera. The ex vitro, "in air" experiments were conducted by placing a coated capsule into a weighing boat which sat on top of the coil.

Dye/drug release experiments were conducted in a similar way, with the capsule totally immersed under the fluid surface. It was held in place by a perforated plastic holder to prevent it floating to the surface. An outlet tube with a nylon mesh filter (to prevent any capsule fragments from entering the tubing) led to a recirculation pump and a flow cell in a spectrophotometer. A return tube carried the fluid back to the tube where the capsule was. Liquid was continually circulated through this loop during the release experiment and absorbance was logged using the spectrophotometer. The readout was fed through an A/D converter and logged by computer. Thermocouples buried in the capsule coating and immersed in the surrounding liquid were used to monitor the temperature. The outputs from these were also logged using the A/D converter (see figure S1.1 and S1.2 for experimental setup).

Instrumentation

Transmission electron micrographs (TEMs) were taken on a JEOL JEM 2000EX microscope at an acceleration voltage of 200 kV. Samples were drop-cast onto carbon-coated 400 mesh copper grids (Agar Scientific Limited, UK). Dynamic Light Scattering (DLS) was measured using a Malvern Zetasizer Nano-ZS. Powder X-ray diffraction (XRD) patterns were recorded on a PanAlytical diffractometer using Co Kα radiation, λ = 1.789010 Å in reflection mode. Differential Scanning Calorimetric (DSC) measurements were recorded on a TA Instruments DSC Q2000 between - 40 and 140 °C. Magnetisation data was taken using a Quantum Design MPMS Super conducting Quantum Interference Device (SQUID) VSM Magnetometer (San Diego, USA) at 300 K using a field range of ±7 T. Hyperthermia experiments were undertaken using a MACH system (Magnetic Alternating Current Hyperthermia) designed and built by Resonant Circuits Limited.[44] The temperature was monitored using a fluoroptic temperature probe (Luxtron FOT Lab Kit, Lumasense California USA). Thermal images were recorded with an Infratec (Germany) VarioCAM HR research 780 with 30 mK thermal resolution and 1280 × 960 spatial resolution. Material

ARTICLE   **Journal Name**

optimisation experiments and drug and dye release experiments in fluids were measured using a Magnatherm Hyperthermia system (a nanoTherics magneTherm™), which for some experiments was linked to a recirculation system and a UV/vis spectrophotometer fitted with a flow cell for monitoring drug release (figure S1.1).

Results and Discussion

Nanoparticle synthesis and characterisation

Iron oxide nanoparticles were successfully synthesised using the aqueous co-precipitation reaction between iron(II) and iron(III) salts in the presence of base.[42] The driving force for this reaction is the formation of solid magnetite Fe_3O_4 and its precipitation from solution. The size of the product can be controlled to a degree by adding surfactant, in this case oleic acid, to the solution, which binds very strongly[45] to growing nanoparticle nuclei and prevents coalescence and the formation of bulk material. In this way, several different batches of iron oxide nanoparticles were obtained with different average sizes, which were characterised by TEM, DLS, XRD and SQUID magnetometry (Figure 1). The different sizes were attributed to the amount of oleic acid used in the synthesis, namely 4 mL, 6 mL, 8 mL and 10 mL.
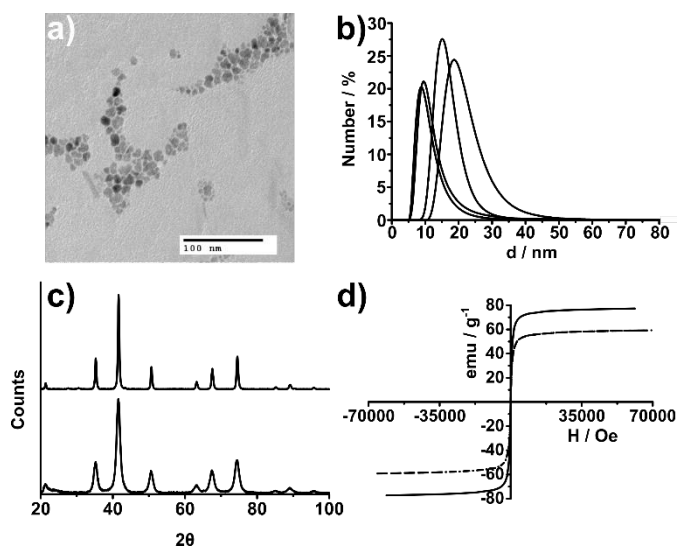

Figure 1: a) TEM micrograph of ~ 10 nm SPIONs, b) DLS number % spectra of 4 mL, 6, mL, 8 mL and 10 mL oleic acid SPION samples, c) XRD patterns of a magnetite (Fe_3O_4) standard (top) and the 8 mL oleic acid SPION sample (bottom) and d) SQUID magnetometry hysteresis loops at 300 K of 4 mL (solid line) and 10 mL (dashed line) oleic acid SPION samples.

TEM analysis gave the sizes of the nanocrystal samples as follows: 8.7 ± 3.8 nm, 6.9 ± 3.1 nm, 5.3 ± 2.7 nm and 3.1 ±

1.6 nm. These were supported by hydrodynamic diameters obtained from DLS analyses in toluene, giving number average size values of: 20.4 ± 1.5 nm, 16.3 ± 2.5 nm, 11.5 ± 1.5 nm and 10.2 ± 2.0 nm for the 4 mL, 6 mL, 8 mL and 10 mL oleic acid samples respectively. DLS and TEM analyses showed a relatively high degree of polydispersity within the sample, as evidenced in figure 1. As is frequently observed for nanoparticles, the sizes measured by DLS for the solvated particles including ligand are approximately double the sizes measured by TEM for the electron-dense cores alone. A degree of shape anisotropy could also account for part of this difference by affecting the DLS size estimates arising from the "equivalent sphere" value produced by fitting to the Stokes Einstein equation. The simplicity of the synthesis method, low cost and scope for scaling up this process to a batch or industrial scale is a key advantage of the co-precipitation method for use in our system and the size range produced provides appropriate functionality.

Powder XRD produced patterns consistent with iron oxide (most likely magnetite Fe_3O_4) (figure 1), with peak broadening attributed to small crystallite size. SQUID magnetometry gave saturation magnetisation values of 77 emu.g^{-1}, 59 emu.g^{-1}, 59 emu.g^{-1} and 58 emu.g^{-1} for each of the nanoparticle samples respectively (superimposed hysteresis loops of 10 nm and 20 nm iron oxide nanoparticle are shown in figure 1). The complete absence of magnetic hysteresis and zero coercivity in any of the samples, coupled with their small size as evidenced by TEM and DLS, indicated that the nanoparticles are superparamagnetic at 300 K. Small superparamagnetic particles were chosen for this work to avoid any possibility of induced residual magnetism (which might occur if the particles were larger and ferromagnetic in nature), which might induce particles to aggregate and hence make them more difficult to disperse and remove from the capsule coating, affecting water ingress and drug release according to the proposed model.

It was found experimentally that, despite the small size of the nanoparticles, they still generated significant magnetic-field induced hyperthermia. The highly non-linear magnetisation curves with large differential susceptibility dm/dH values evident in these plots would not normally be seen for such small particles if they were monodisperse, but these samples are significantly polydisperse, giving rise to the observed behaviour and consistent with the size characterisation data (see figure 1). It is probable that the polydispersity also explains the range of magnetic field strengths and frequencies that could be employed to give efficient heating, since the power loss from these single domain particles is dictated by matching the relaxation time of particles to the frequency and applied field[9]. A heterogeneous population will ensure that some part of the population is well matched to the conditions even when the frequency is changed. It is also probable that some clustering/aggregation of particles takes place, both in solution and in the wax-composites (see later), where loading and hence proximity will be high. Inter-particle interactions can have a

dramatic effect on the efficiency of magnetic-field induced heating[46].

Capsule coating

The ideal material for a capsule coating has to conform to certain constraints and possess a wide range of attributes. The material has to be biologically inert and non-toxic, as well as exhibiting normal melting behaviour. Nanoparticle dispersibility in organic solvents is also desirable to ensure an even coverage throughout the coating. Crucially, the melting point of the material has to be above physiological temperature (> 37 °C), but not so high that the molten capsule causes internal tissue damage (assuming such a temperature could be reached). Therefore, two different temperature-tunable wax systems were investigated for making the nano-composite materials: eicosane, docosane, eicosane-docosane mixtures and a fatty acid mixture comprising myristic and lauric acids.
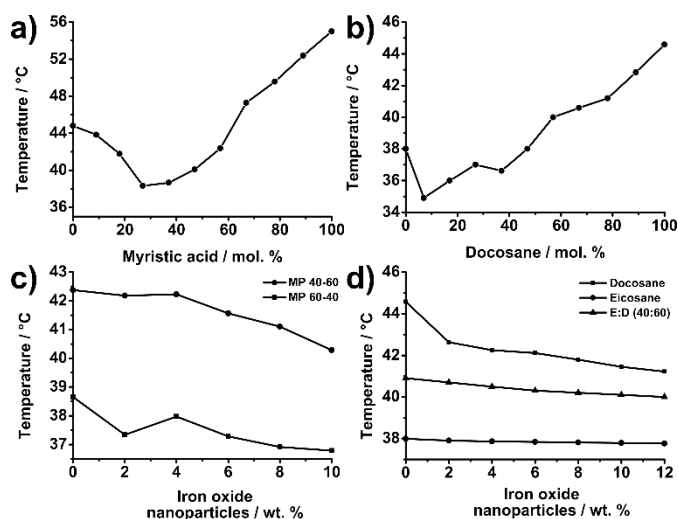

Figure 2: Variation in melting temperature (measured by DSC) of a) a mixture of myristic acid and lauric acid (FA) mixture with increasing myristic acid mol. %, b) melting temperature variation in an eicosane-docosane mixture, c) melting temperature variation in a SPION loaded FA mixture and d) melting temperature variation in SPION loaded eicosane, docosane and eicosane:docosane (40:60 mixture).

Eicosane ($C_{20}H_{42}$) and docosane ($C_{22}H_{46}$) are aliphatic hydrocarbons with melting points of 40 °C and 45 °C respectively (midpoint values from DSC – see figures S5.4 and S5.5). These hydrocarbons were selected because of their biological inertness, affinity with oleic acid stabilised nanoparticles and melting points. Although the melting point of eicosane is very close to body temperature and the melting point of docosane is high enough to cause tissue damage, it was found that a mixture of these two compounds could be tuned

by varying the composition to give a range of useful melting points, as evidenced by summarised DSC measurements (Figure 2). A mixture of myristic acid ($C_{13}H_{27}COOH$, m.p. 56.7 °C) and lauric acid ($C_{11}H_{23}COOH$, m.p. 44.6 °C) was also chosen as a biologically compatible material with a melting point in the correct range (figures S5.1-S5.3).

All materials performed well during the synthesis stage, forming a homogeneous dispersion with iron oxide nanoparticles at *ca.* 60 °C, with little difficulty in preparing a defect-free capsule *via* dip-coating (Figure 3 e) and f)). The gelatin capsules were immersed into a molten dispersion of wax-nanoparticle liquid via a suction tube, with the layer of wax cooled before subsequent immersion steps. The thickness of the coatings was analysed by optical microscopy of coating cross-sections. The hydrocarbon waxes produced smoother and more even coatings than the fatty acid mixtures. Addition of nanoparticles to the wax mixtures caused a small depression of the melting points of the composites, which increased with particle loading, presumably due to disruption chain packing. This required the compositions to be adjusted slightly to achieve the target melting temperature, but up to the 10 wt. % limit tested, there was no obvious effect on coating integrity or dissolution behaviour (figure 3).
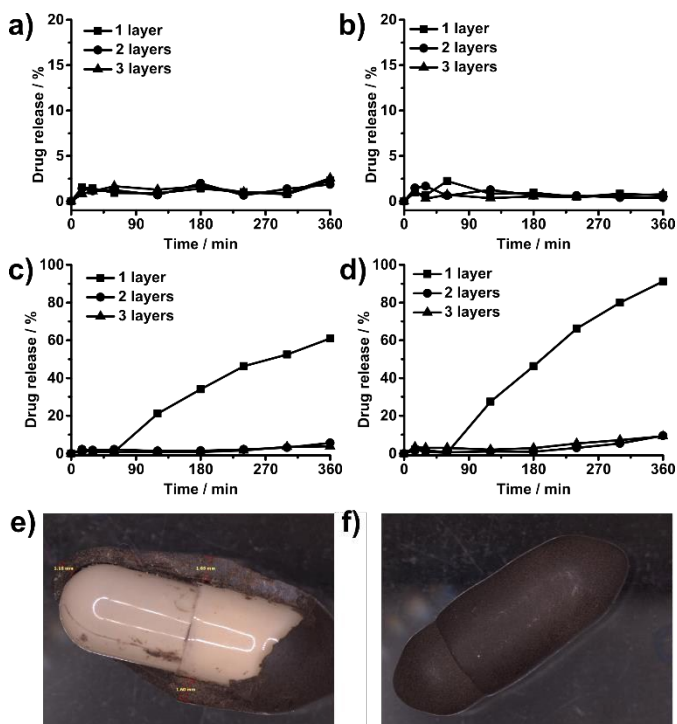

Figure 3: Integrity testing results of an eicosane coated capsule in a) aqueous solution pH ranges 1.2-7.4 mimicking transit through the GI tract and b) in pH 1.2 then FaSSIF buffer pH6.5 and 37 °C. c) and d) show the same measurements on a mixture of lauric and myristic acid (40:60 ratio w/w). e) and f) are photographs of coated capsules, with e) showing coating thickness.

Dissolution testing

Dissolution testing in intestine-mimicking conditions showed that a single layer of fatty acid was insufficient to protect the capsule and drug release began during the two hours of incubation in HCl pH 1.2 (mimicking the stomach). Thicker layers were more protective, but even then the fatty acid coating was compromised by incubation under mildly alkaline conditions (most likely due to ionisation and dissolution of the fatty acids), leading to slow leakage of drug during the intestine mimicking phase. The coatings composed of eicosane and docosane proved to be robust in immersion testing and resistant to changes in pH required for GI tract drug delivery (Figure 3).

Hyperthermia behaviour

The ability of the SPIONs to cause hyperthermic heating was tested using the Magnatherm instrument at a range of different frequencies and field strengths for particles of different sizes (figure 4). All six frequencies available with the Magnatherm instrument (between 110 and 737 kHz) and particle size combinations tested (24 in all) caused heating, but there were differences in the rates of heating and the final temperatures achieved due to the efficiency of magnetic coupling. The most efficient combination was 521.3 kHz (24 mT field strength), combined with the smallest (~10 nm) particles, so these conditions were adopted for subsequent wax and capsule heating studies.
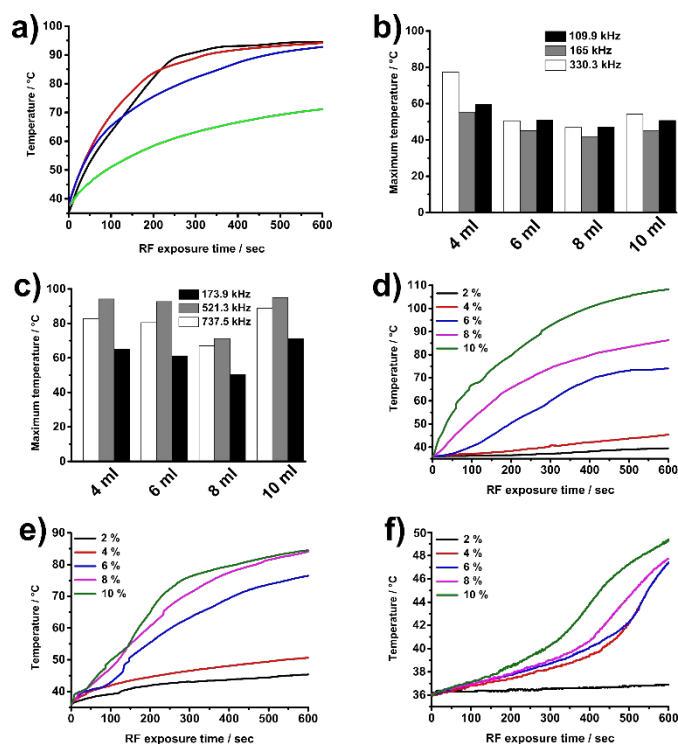

Figure 4: a) Temperature maxima of 4 ml (red), 6 ml (blue), 8 ml (green) and 10 ml (black) oleic acid SPION samples in water as a function of RF exposure time giving an indication of a rapid response at 521.3 kHz with a 9 turn coil. b) (17 turn coil) and c) (9 turn coil) show temperature maxima attained by the indicated SPION samples in water over 600 seconds at different frequencies. d), e) and f) are different heating curves and melting behaviours of bulk eicosane, eicosane-docosane and fatty acid SPION composites respectively at 330.3 kHz at different nanoparticle loadings. The 10 ml oleic acid SPION sample (average size 10.2 nm) was used for the shown experiments. The temperatures were logged at 1s intervals using a T-type thermocouple inserted into the sample, which was connected to an A/D converter.

Initial hyperthermia testing of wax-SPION composites focused on nanoparticle loading (Figure 4d), e) and f)). 2 wt.% nanoparticle loading caused almost no heating when encapsulated in the fatty acid mixture, but as the loading increased the rate of heating increased markedly and the solids melted. It is interesting to note the lag phase in the heating curves when the nanoparticles were in the solid phase. Once the melting temperature was attained and the solid changed phase, the heating rate was markedly higher. This presumably represents the transition from Néel heating alone in the solid to Néel and Brownian heating once in the liquid state where Brownian motion is no longer restricted.[47] Similar behaviour was noted for the hydrocarbon waxes (see figure S6). The important point is that melting of the composites was easily attained through RF heating within 1-2 minutes with a 10 wt.%

nanoparticle loading, thus demonstrating the viability of the proposed release trigger.

Capsule heating through magnetic field-induced hyperthermia

In order to visualise the process of capsule heating and melting, various capsule coating formulations were tested using the MACH hyperthermia rig. This allowed RF exposure, while recording the capsule using a high resolution thermal imaging camera. Some typical results from this study are shown in Figure 5 (further results and videos from the thermal imaging camera are available in ESI). The recorded heating curves in air for fatty acid, eicosane and eicosane/docosane are shown in panel (a). Two points are immediately clear from these results. Firstly, the pronounced biphasic behaviour discussed above is clearly visible as the capsule coatings start off in the solid state and then go through a melting transition, whereupon the heating rate dramatically increases. Secondly, the heating and melting of the fatty acid coated capsule appears to be much more difficult. During the time-frame of the experiment the coating never fully melted and the rapid increase in the temperature seen for the hydrocarbons did not occur. It is not clear what causes this dramatic difference, since DSC measurements suggested that the fatty acids and the hydrocarbon waxes had similar values for the latent heat of melting and the layer thicknesses were similar. It is possible that some phase separation and crystallisation has occurred and that only melting of the C12-rich phase is being observed, which does not lead to complete layer melting. The visual capsule images confirm that some liquid material is visible at the end of the experiment (figure 5(i)), but the coating overall is still intact. Experiments carried out with the capsule partly or wholly submerged in FaSSIF buffer also showed some leaching of brown iron-oxide containing material into the buffer, but dye release from the gelatin capsule was not observed (see figure S4). By contrast, the hydrocarbon coatings heated and melted rapidly, again showing the biphasic shape as the material passed through the solid liquid phase transition, before rapid heating of the liquefied coating to high temperature. Experiments with partially and wholly submerged capsules showed release of dye from the capsule interior, confirming that melting of the coating triggered release of the capsule contents as predicted.

Figure 5 demonstrates the maximum temperatures achieved over different time periods in air, with capsule coatings attaining high temperatures (not seen under immersion in liquid systems (figure 6) which have high specific heat capacity, "buffering" the hyperthermic heating). These high temperatures are not required for capsule coating melting, water ingress and ultimately drug release, but figure 5 is designed to demonstrate the rapid hyperthermia-activated trigger for drug release in our system.
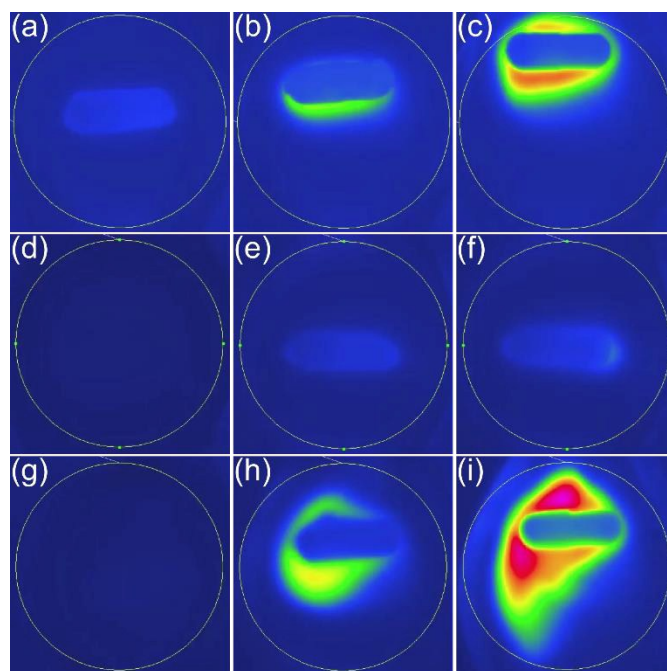

Figure 5: Thermal images of the coated capsules in the presence of the alternating magnetic field. The drawn circle surrounding the capsule indicates the position of the RF coil. Top 3 images are of the eicosane-SPION coated capsule at time t = (a) 30 s, (temperature maximum 35.43 °C) (b) 90 s, (temperature maximum 37.33 °C) and (c) 210 s, (temperature maximum 64.54 °C). Middle 3 images are of the fatty acid-SPION coated capsule at time t = (d) 0 s, (temperature maximum 29.03 °C) (e) 30 s, (temperature maximum 37.18 °C) and (f) 90 s, (temperature maximum 44.77 °C). Bottom 3 images are of the eicosane-docosane-SPION coated capsule at time t = (g) 0 s, (temperature maximum 29.23 °C), (h) 30 s, (temperature maximum 67.49 °C) and (i) 90 s, (temperature maximum 99.26 °C).

Dye/drug release experiments

To demonstrate drug release under simulated gut conditions, a rig was constructed around the Magnatherm instrument, which maintained the capsule immersed in a thermally-equilibrated buffer reservoir, while recirculating fluid from the reservoir through a spectrophotometer to monitor paracetamol release via its UV absorbance. A typical result for an eicosane/docosane coating is shown in figure 6. The temperature of the capsule coating was monitored *via* a thermocouple embedded in the coating layer (inserted at the time of coating when the layer was still soft). A second thermocouple monitored the temperature of the surrounding buffer.

Capsules were loaded with bromo-cresol green or paracetamol and coated with iron oxide nanoparticle-wax following the aforementioned procedure. These experiments were designed to provide confirmation of the ability of a

ARTICLE

capsule to retain a dye whilst forcibly submerged in an aqueous environment and then to release it once triggered.

A thermocouple was placed in the coating of the capsule to measure temperature increases and signify melting, whilst the temperature of the aqueous environment and drug release (by in situ UV/vis spectroscopy) were also recorded. The results of these experiments can be found in Figure 6 a) and b), with eicosane coated capsules containing paracetamol exposed to radiofrequencies of 330.3 kHz and 521.3 kHz respectively. The SPION loading of the eicosane coating was kept at 10 wt. % for all experiments and coating types, graphs of which can be found in the ESI (figure S2 and S3).

Each of the coatings under scrutiny showed a sharp content release once the capsule coating had started to melt, and no capsule coating took more than 800 seconds of exposure time to effect complete drug release. Different radio-frequencies and capsule coatings employed demonstrate the extreme versatility of our drug delivery technology for rapid and on-demand drug release.

It is noteworthy that the magnetic-field induced heating was localised almost entirely to the capsule coating, with the temperature of the surrounding environment never rising above 38 °C, thus avoiding collateral tissue damage. The dip in the temperature profile after about 100 s from the thermocouple embedded in the wax coating is probably due to localised melting causing movement and possible partial detachment of the thermocouple. The increase in temperature of the surrounding medium is due to the enclosed environment and the fact that the capsules were heated until the coating had completely melted. Some heat transfer occurs from the capsule to the environment, but thermal diffusion from the RF coil was minimised by balancing the recirculating cooling water such that in the absence of SPIONS a constant temperature of 37 °C was maintained under RF load. Shorter induced heating times (and lower temperatures) than those in figure 5 are required to achieve sufficient melting of the capsule coating to ensure content release, with the majority of time taken required for the fluid ingress necessary to dissolve the gelatin capsule and release the drug, as shown in the traces in figure 6. It appears that about two minutes of RF heating cause sufficient melting/disruption to lead to eventual release of the capsule contents.
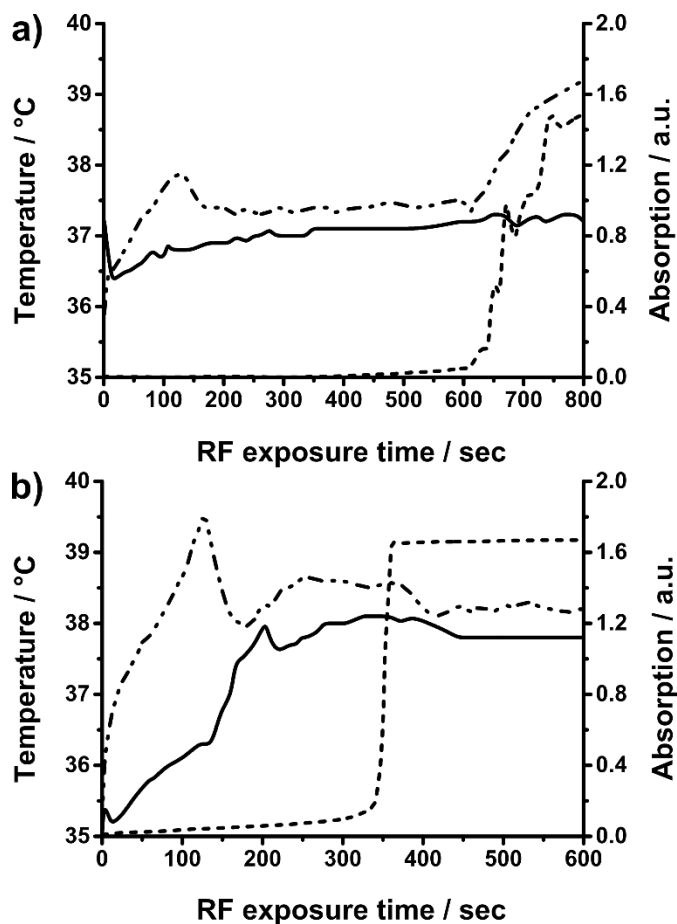

Figure 6: Paracetamol release from eicosane capsules with a 10 wt. % SPION loading at a) 330.3 kHz and b) 521.3 kHz. The solid line is the temperature of the medium (i.e. buffer surrounding the capsule), the short dash line is the UV trace signalling at what point the paracetamol was released through an increase in absorption and the dot-dashed line is the temperature of the capsule measured by an incorporated T-type thermocouple.

The nature of the dye release also illustrated that only a small area of capsule exposure to the surrounding environment is required and may be beneficial for improving drug targeting. Indeed, more sophisticated, second generation capsule coatings could potentially only require a small area to be sensitive to the hyperthermia trigger (e.g. to unlock the channel to an inbuilt osmotic pump), for greater control over drug release and reduced *in vivo* quantity of nanomaterial required.

Conclusions

The development and optimisation of an effective, yet simple iron oxide nanoparticle-wax composite coating for magnetic hyperthermia-triggered drug delivery in the GI tract has been demonstrated. Several coating compositions have been

evaluated for their robustness to the chemical and mechanical conditions experienced within the GI tract. It is also noteworthy that the materials used to synthesise the capsules and capsule coatings are pharmaceutically approved (i.e. all the chemicals used are listed in the British Pharmacopoeia either as medications in their own right (e.g. ferrous sulphate B.P. for treatment of anaemia), as components of other medications (e.g. oleic acid in emulsions and ointments) or in less refined forms (e.g. eicosane is a component of white soft paraffin/petroleum jelly).

Dissolution and magnetic hyperthermia release studies were successful for all nanoparticle sizes and waxy surface coatings, although the mixture of fatty acids was shown to be degraded by alkaline environments, analagous to those experienced in the intestinal tract. However, it was demonstrated that the hydrocarbon coatings were not compromised over 72 hours, well over typical intestinal transit time.

Acknowledgements

Notes and references

1   G. Brakmane, M. Winslet and A. M. Seifalian, *Aliment. Pharmacol. Ther.*, 2012, **36**, 213–221.

2   D. Vyas, P. Castro, Y. Saadeh and A. Vyas, *J. Biomed. Nanotechnol.,* 2014, **10**, 3204–3218.

3   F. Talaei, F. Atyabi, M. Azhdarzadeh, R. Dinarvand and A. Saadatzadeh, *Eur. J. Pharm. Sci.*, 2013, **49**, 712–722.

4   C. Lautenschläger, C. Schmidt, D. Fischer and A. Stallmach, *Adv. Drug Deliv. Rev.*, 2014, **71**, 58–76.

5   J. Shi, A. Votruba, O. Farokhzad and R. Langer, *Nano Lett.*, 2010, **10**, 3223–3230.

6   C. X. Song, V. Labhasetwar, H. Murphy, X. Qu, W. R. Humphrey, R. J. Shebuski and R. J. Levy, *J. Controlled Release*, 1997, **43**, 197–212.

7   D. Guarnieri, A. Falanga, O. Muscetti, R. Tarallo, S. Fusco, M. Galdiero, S. Galdiero and P. A. Netti, *Small*, 2013, **9**, 853–862.

8   L. Brannon-Peppas and J. O. Blanchette, *Adv. Drug Deliv. Rev.*, 2004, **56**, 1649–1659.

9   T. Neuberger, B. Schöpf, H. Hofmann, M. Hofmann and B. von Rechenberg, *J. Magn. Magn. Mater.*, 2005, **293**, 483–496.

10 J. Bear, G. Charron, M. T. Fernández-Argüelles, S. Massadeh, P. McNaughter and T. Nann, in *BetaSys: Systems Biology of Regulated Exocytosis in Pancreatic ß-Cells*, Springer New York, 2011, vol. 2, pp. 185–220.

11 L. Gu, R. H. Fang, M. J. Sailor and J.-H. Park, *ACS Nano*, 2012, **6**, 4947-4954.

12 A. M. Smith, H. Duan, A. M. Mohs and S. Nie, *Adv. Drug Deliv. Rev.*, 2008, **60**, 1226–1240.

13 J. Park, P. M. Fong, J. Lu, K. S. Russell, C. J. Booth, W. M. Saltzman and T. M. Fahmy, *Nanomedicine Nanotechnol. Biol. Med.*, 2009, **5**, 410–418.

14 C. Sun, K. Du, C. Fang, N. Bhattarai, O. Veiseh, F. Kievit, Z. Stephen, D. Lee, R. G. Ellenbogen, B. Ratner and M. Zhang, *ACS Nano*, 2010, **4**, 2402–2410.

15 X. Zhang, P. Yang, Y. Dai, P. Ma, X. Li, Z. Cheng, Z. Hou, X. Kang, C. Li and J. Lin, *Adv. Funct. Mater.*, 2013, **23**, 4067–4078.

16 S. Chen, Y. Li, C. Guo, J. Wang, J. Ma, X. Liang, L. Yang and H. Liu, *Langmuir*, 2007, **23**, 12669–12676.

17 Q. Yuan, R. Venkatasubramanian, S. Hein and R. D. K. Misra, *Acta Biomater.*, 2008, **4**, 1024–1037.

18 F. Caruso, M. Spasova, A. Susha, M. Giersig and R.A. Caruso, Chem. Mater. 2001, **13,** 109-116

19 A. Lamprecht *Nature Reviews Gastroenterology and Hepatology* 2010, **7**, 311-312

20 A. Lamprecht *Nature Reviews Gastroenterology and Hepatology* 2015, **12**, 195-204

21 H. Wen and K. Park (eds.) Oral Controlled Release Formulation, Design and Drug Delivery – Theory and Practice. John Wiley and Sons, 2011.

22 T. Bussemer, I. Otto and R. Bodmeier *Critical Reviews in Therapeutic Drug Carrier Systems*, 2001, **18,** 433-458

23 V.R. Sinha and R. Kumria *Eur J. Parm. Sci.* 2003, **18**, 3-18

24 N.M. Kasekar, G.J.C. Gupta, K.J. Jadhaw, S. Aiyer andV.J. Kalam, *World Journal of Pharmacy and Pharmaceutical Sciences* 2014, **3**, 580-603

25 J. Liu, Y. Huang, A. Kumar, A. Tan, S. Jin, A. Mozhi and X.-J. Liang, *Biotechnol. Adv.*, 2014, **32**, 693–710.

26 K. S. Soppimath, D. C.-W. Tan and Y.-Y. Yang, *Adv. Mater.*, 2005, **17**, 318–323.

27 Y. Yu, C.-K. Chen, W.-C. Law, E. Weinheimer, S. Sengupta, P. N. Prasad and C. Cheng, *Biomacromolecules*, 2014, **15**, 524–532.

28 Z. B. Starkewolf, L. Miyachi, J. Wong and T. Guo, *Chem. Commun.,* 2013, **49**, 2545–2547.

29 C. S. S. R. Kumar and F. Mohammad, *Adv. Drug Deliv. Rev.*, 2011, **63**, 789–808.

30 Y. Chen, A. Bose and G. Bothun, *ACS Nano*, 2010, **4**, 3215–3221.

ARTICLE

31 T. Atsumi, B. Jeyadevan, Y. Sato and K. Tohji, *J. Magn. Magn. Mater.,* 2007, **310**, 2841–2843.

32 L. A. Thomas, L. Dekker, M. Kallumadil, P. Southern, M. Wilson, S. P. Nair, Q. A. Pankhurst and I. P. Parkin, *J. Mater. Chem.*, 2009, **19**, 6529.

33 J. C. Bear, B. Yu, C. Blanco-Andujar, P. D. McNaughter, P. Southern, M.-K. Mafina, Q. A. Pankhurst and I. P. Parkin, *Faraday Discuss.,* 2014, **85**, 83-95.

34 A. E. Deatsch and B. A. Evans, *J. Magn. Magn. Mater.*, 2014, **354**, 163–172.

35 R. Hergt, R. Hiergeist, I. Hilger, W. A. Kaiser, Y. Lapatnikov, S. Margel and U. Richter, *J. Magn. Magn. Mater.*, 2004, **270**, 345–357.

36 D. R. Friend, *Adv. Drug Deliv. Rev.*, 2005, **57**, 247–265.

37 Friend, *Aliment. Pharmacol. Ther.*, 1998, **12**, 591–603.

38 S. Laurent, D. Forge, M. Port, A. Roch, C. Robic, L. Vander Elst and R. N. Muller, *Chem. Rev.*, 2008, **108**, 2064–2110.

39 B. P. Commission, British pharmacopoeia 2015, Stationery Office, London, 2014.

40 I. Baker, Q. Zeng, W. Li and C. R. Sullivan, *J. Appl. Phys.*, 2006, **99**, 08H106–08H106–3.

41 R. Hergt and S. Dutz, *J. Magn. Magn. Mater.*, 2007, **311**, 187–192.

42 M. T. López-López, J. D. G. Durán, A. V. Delgado and F. González-Caballero, *J. Colloid Interface Sci.*, 2005, **291**, 144–151.

43 E. Galia, E. Nicolaides, D. Hörter, R. Löbenberg, C. Reppas and J. B. Dressman, *Pharm. Res.*, 1998, **15**, 698–705.

44 http://resonantcircuits.com/.

45 M. Lattuada and T. A. Hatton, *Langmuir*, 2007, **23**, 2158–2168.

46 C. Blanco-Andujar, D. Ortega, P. Southern, Q.A. Pankhurst and N.T.H. Thanh, Nanoscale, 2015, 7, 1768-1775

47 D. Yi, P. Zeng and T. S. Wiedmann, *Int. J. Pharm.*, 2010, **394**, 143–146.